Heliyon 10 (2024) e31769

Contents lists available at ScienceDirect

Heliyon

journal homepage: www.cell.com/heliyon

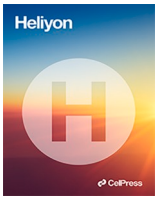

Research article

A novel procedure for medial axis reconstruction of vessels from Medical Imaging segmentation

C. Fontana *, N. Cappetti

Department of Industrial Engineering, University of Salerno, Fisciano, SA, 84084, Italy

ARTICLE INFO

Index Terms:
Medial axis
Vessel reconstruction
Morphological analysis
Medical Imaging

ABSTRACT

A procedure for reconstructing the central axis from diagnostic image processing is presented here, capable of solving the widespread problem of stepped shape effect that characterizes the most common algorithmic tools for processing the central axis for diagnostic imaging applications through the development of an algorithm correcting the spatial coordinates of each point belonging to the axis from the use of a common discrete image skeleton algorithm.

The procedure is applied to the central axis traversing the vascular branch of the cerebral system, appropriately reconstructed from the processing of diagnostic images, using investigations of the local intensity values identified in adjacent voxels. The percentage intensity of the degree of adherence to a specific anatomical tissue acts as an attraction pole in the identification of the spatial center on which to place each point of the skeleton crossing the investigated anatomical structure.

The results were shown in terms of the number of vessels identified overall compared to the original reference model.

The procedure demonstrates high accuracy margin in the correction of the local coordinates of the central points that permits to allocate precise dimensional measurement of the anatomy under examination.

The reconstruction of a central axis effectively centered in the region under examination represents a fundamental starting point in deducing, with a high margin of accuracy, key informations of a geometric and dimensional nature that favours the recognition of phenomena of shape alterations ascribable to the presence of clinical pathologies.

1. Introduction

1.1. Context

The recognition of suspicious phenomena from the interpretation of diagnostic images usually relies on the identification of alterations in the spatial arrangement and structural conformation of the case under investigation. A modern approach to the diagnostic problem intends to automate the processing pathway, employing software tools capable of characterising the morphology of the anatomical region, and identifying parameters that can lead to the recognition of pathological alterations. In the biomedical field, in particular, this type of procedure is widely used in the three-dimensional analysis of multiple anatomical regions; one example

* Corresponding author.
E-mail address: cfontana@unisa.it (C. Fontana).

https://doi.org/10.1016/j.heliyon.2024.e31769
Received 24 July 2023; Received in revised form 9 May 2024; Accepted 21 May 2024
Available online 23 May 2024

concerns the identification of lobes in the liver area [1] and the study of cranial and optic nerves [2,3]. Not infrequently, it also makes it possible to discriminate between different diagnoses, accurately describing the structure of a particular anatomical anomaly [4]. A further application case of form functions is that of rapid prototyping [5] and 3D navigation [6]. One of the most significant areas of application concerns the identification of potential risk factors from the observation of the spatial arrangement of vascular branches, in which an early diagnosis can be decisive in drafting a correct surgical procedure [7,8].

In the context of the clinical elaboration of anatomies with threadlike conformation, as in the case of vascular structures, it is extremely effective to use a procedure of morphological reduction of the case study to its central axis, suitably reconstructed through the use of widespread shape algorithms [9–12]. A procedure common to modern approaches to the problem examines the structural conformation of the case under examination starting from the reconstruction of its central axis, which, by its nature, preserves the topological connotations of the reference anatomy. To the reconstruction of the central axis are, therefore, attributed geometric and dimensional informations, the interpretation of which is the object of study in clinical examination. Over the years, the scientific community has produced countless numbers of highly accurate center-axis reconstruction algorithms, resulting in different computational methods, each distinguished by its own special optimization technique. Most applications return a central axis whose spatial arrangement corresponds to a precise location within the distribution of voxels of which the source diagnostic image is composed. Its dependence on the spatial discretization that characterizes digital images can, however, lead to the potential occurrence of errors in the extrapolation of dimensional and topological information of the anatomy under investigation from the processing of its central axis. The present research work intends to propose a *smoothing* procedure of the central axis, suitably reconstructed from the use of traditional methods, which returns a new spatial ordering of the identified points, eliminating the grooved effect that normally characterizes discrete central axes. The spatial relocation criterion employed is based on the observation of the local intensity levels of the voxels, expressed in Hounsfield scale, representative of the occupational level of a specific anatomical region. The observation of the local values can influence the positioning of each point on the central axis, acting as attractive poles capable of returning a correct reconstruction of the morphology and topology of the anatomical region under investigation.

1.2. State of the art

An explanatory survey of the main methods of reconstructing the central axis is described by Saha et all [13]. More generally, the most accredited procedures for the reconstruction of the central axis of diagnostic anatomies can be traced back to two approaches: the first one processes the original raw image composed by voxel sequences; the second one disregards discrete space through the use of triangularization procedures of the outer anatomical surface. Regardless of the type of approach used, the analytical procedures for developing the central axis can be divided into three main categories, summarized below:

Erosion propagation algorithm: An erosion front represents an elementary methodology for reconstructing the distance function from an erosion process of the surface edges of the region under investigation. This procedure was first introduced by Blum [14] explained through the procedural analogy of a fire propagating front from the edges of a surface. The joining element of the two fronts is precisely the representation of the central axis of the starting figure [15,16]. This formulation can be easily integrated into the three-dimensional environment by considering the third dimension when calculating the distance [17].

Center of Maximall Spheres algorithm: The most widely recurring definition of *Medial Axis* in three-dimensional shape analysis procedures trace back to the *Maximum Ball* algorithm, defined as the computation of the maximum number of spheres inscribed within the model under consideration.

If we consider a triangularized or discrete surface [18], the central axis is derived from the centers of only the 'maximum' inscribable spheres in the volume under consideration, whereby the remaining possibly calculated but non-maximum spheres are ignored in the final selection process.

In the context of reconstructing the central axis from inscribable spheres, the center of the identified sphere represents a point on the central axis and its radius value represents a local measure of the distance function.

Graph-type geometric processing algorithm: Throughout the field of medial axis processing by means of a graph generation method, the *Voronoi* diagram represents an extremely recurrent and effective reconstruction algorithm, in which, starting from a set n of sample points, the environment is divided into an equal number of convex polygonal elements such that each polygon contains exactly one generator point and each point in a given polygon is closer to its generator point than to any other [19]. The *Voronoi* diagram is frequently used in every field of science. In diagnostic image analysis, in particular, some of the main uses of this methodology concern the distribution of anatomical space according to a correct segmentation procedure [17] for the design of prosthetic implants [20] together with morphological analyses. Even the reduction of three-dimensional elements to their central axis, as is the case with skeletonization, is not infrequently entrusted to a Voronoi-type spatial division [21,22]. The skeletonization procedure using the *Voronoi* diagram involves constructing the central axis using a series of sample points from elements belonging to the contour of the region of interest. Downstream of the spatial partitioning, the polygonal segments within the region are considered as skeleton segments. The fundamental limitation of a skeletonization tool of this type is the strong dependence on the number of sample points selected in the initial phase. As this number increases, in fact, the number of branches constituting the skeleton increases, ineffective for the purposes of reconstructing the central axis of the figure alone. An optimization procedure therefore involves identifying the correct number of initial points to generate the ideal central profile [23].

A classification of the criteria for assessing the degree of skeletal accuracy obtained by applying the foregoing methods is listed by Tagliasacchi [24], and makes it possible to compare results from different skeletonization. They can be applied to different starting geometries with a certain interchangeability, are them in a discretized or triangularized form, which is since they generally lead to results that can be considered similar in three-dimensional models that are not too complex.

Disecretized models from medical Digital images condition the behaviour of the skeletonization methods, whose optimization procedure requires different and not always effective attention. The problems linked to this area are many and concern resolution problems intrinsically related to the extraction of dimensional information starting from a discrete digital image, which inevitably affect the precision of reconstruction of the central axis, both starting from the discrete element as a result of a segmentation process, or following an attempt at surface leveling, through the use of triangularization processes.

In the context of the use of discrete geometries, the first comprehensive description of the problem was addressed by Tsao [25] who applies an erosive, parallel-type skeletonization process to three-dimensional elements. The results of this work make it possible to clarify the limiting factors to be considered when writing such algorithms, such as 'topological connectivity constraints' together with 'non-topological shape criteria'.

Some of these procedures have been implemented and are also applied within already widely consolidated tools which make up important diagnostic image processing software, as is the exemplary case of Mimics (MaterialiseMimics®), for investigations which contemplate the reconstructive use of the central axis as in Ref. [26].

With reference to the computational structure, we can trace the skeletonization procedures applied to discrete images to the recurrent use of erosion-type approaches, throughout *kernel* matrices, in which the possibility of removing a given *voxel is* established, starting from both topological and morphological reference conditions [27,28]. This skeletonization procedure is highly effective, if it is 'tailor-made' with respect to the physical characteristics of the object under investigation, leading to *overfitting* problems, due to the lack of versatility in response to very different geometries. A second category of algorithms relates to the possibility of extracting information on the central axis of a discrete figure, using the distance function directly. In fact, the latter contains information on the point distance of each element from the edge, which makes it possible to identify the axis through the identification of an area of symmetry in the distribution of distances [29–31]. This type of formulation appears extremely efficient from a computational point of view, being robust with respect to rotation. It becomes more problematic in a parallelization condition.

The irregularities resulting from the processing of discrete surfaces can be remedied by using a smoother external surface as an input. One way of achieving this is by performing a triangularization procedure for reconstructed anatomical volumes. The conversion of a three-dimensional scalar field, composed of *voxels,* into a polygonal *mesh is* called 'Marching Cubes'. This is an algorithm developed specifically in the biomedical field to facilitate the 3D visualization of CT and MRI devices [32].

The triangularization of a *voxel* sequence leads to the problem of identifying the correct position to assign to the vertex that replaces the *voxel it* belongs to. This is normally placed at the center of the elementary cube, or of a relative intersecting edge, or sometimes at an extreme vertex of the same, as in Fig. 1.

In the determination of vertex coordinates, what ensues is an approximate reconstruction of the surface of the region under examination to which shape functions, including that relating to the central axis, are applied. A way of overcoming inaccuracies in reconstruction could be to locally thicken voxels, corresponding to regions where the proximity of the contour to a neighboring vertex of the voxel is not defined. This solution, however, is not without its errors, which are also followed by a non-negligible computational effort in assessing the overall effectiveness of the algorithm. The application of central axis generation algorithms starting from triangularized geometries is able to overcome discretization problems, resulting in a positioning of the axial reference points spatially distributed in a generally more uniform and homogeneous way. The approximation resulting from the triangularization process, however, is not free from producing some geometric precision errors.

Comparison of skeletons: differences between discrete geometries (voxels) and triangularized geometries (point clouds).

Following the aforementioned clarifications relating to the most representative methods in the reconstruction of the central axis

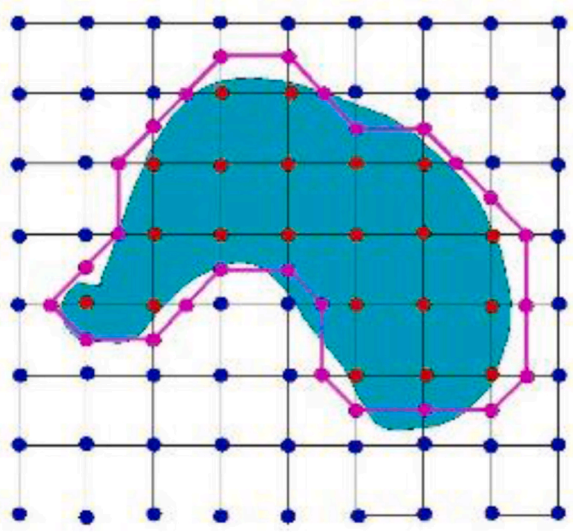

Fig. 1. Representative image of a triangularization procedure applied to a two-dimensional case [33].

from diagnostic images, it is appropriate to identify the most significant salient points in comparison with the use of one or the other geometric shape considered.

As previously denoted, the skeletonization of a geometry in voxel form is extremely invariant to isometric transformations, unlike triangularized elements.

On the other hand, however, a volume distribution of discrete elements produces, in its skeletonization, a central element whose spatial continuity is staggered, in the form of a stepped configuration, and, therefore, almost never perfectly centered.

Finally, we note the inaccuracy generated by the reproduction of the axis in discrete models, whose points are, as a rule, centered in the voxel or one of its vertices, leading to errors in dimensional reconstruction and, in extreme cases, the exclusion of certain zones in the crossing of the central skeleton.

A representation of the central axis from meshes, however, more frequently incurs the generation of superfluous branches, unsuitable for representing the skeleton alone, necessitating the development of optimization methods, which go by the name of pruning algorithms [34,35].

A critical analysis of the application results of the main center-axis reconstruction algorithms reveals a large margin of error due to the implication of using discrete volumes. This approximate condition suggests investigating an algorithmic optimization method capable of improving the positioning of the central axis, respecting the topological characterization of the diagnostic image which is the starting point of the analyzes for identifying the correct morphology of the blood vessels intracranial for the applications discussed in the introduction.

The purpose of this research work is to evaluate the efficacy of an algorithm for reconstructing the central axis of the cerebral vessels of the intracranial region. This algorithm improves the medial axis on discrete models (voxels). Compared to those described, with the aim of increasing the degree of accuracy in the geometric positioning of the axis, reducing the stepped shape effect and preserving the originality of the starting diagnostic source and limiting the intervention of approximate manipulation forcibly generated by a triangularization process.

2. Material and methods

2.1. Case study: reconstruction of the central axis of cerebral vessels

Evaluations of the effectiveness and quality of the medial axis obtained with the algorithm proposed in this paper will be based on the elaborations carried out on a triangularized atlas model of the Willis Polygon [36], available in the literature, which is representative of the main vascular branch to which the blood supply to the head is entrusted (Fig. 2). This system of vessels is representative of a structure made up of roughly tubular elements, branching out along different spatial orientations with different degrees of curvature and tortuosity and the size of the vessels almost comparable with that of the voxels and represents an extremely significant test since it contains all the critical elements (direction, size, curvature, branches) on which existing methods of skeletonization of discrete models have shown not to perform well [37].

The medial axis obtained from the triangularized model will be used as a comparison reference to evaluate the quality and critical issues of the medial axis obtained with our algorithm.

The decision to take this model as a reference stem from the need, which emerged from the study of the foregoing methodologies described in the state of the art, to identify a reference 'Gold Standard' to be used in the validation of the level of accuracy of the results obtained downstream of the application of the diagnostic image processing functions.

For this reason, the reference model was appropriately discretized into voxels. The reconstruction of the relative central axis can then be obtained, in order to characterize the different behaviour exhibited by the main algorithms employed by the scientific community as the morphological and topological characteristics of the starting geometries vary. The result of the discretization on the reference model is illustrated in Fig. 3.

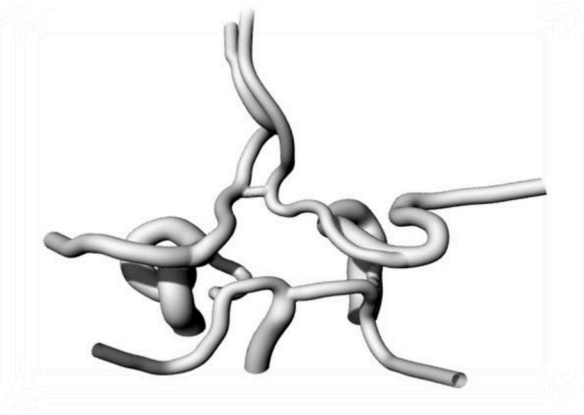

Fig. 2. Atlas model of the Circle of Willis in mesh format used for Medial Axis correction checks.

The validation of a volume discretization tool in voxels, together with a comparative comparison of the most common center-axis reconstruction algorithms, also known as Medial Axis algorithms, represented the core development of the present research work, aimed at experimenting with the development of a procedure for optimizing center-axis reconstruction, obviating the inaccuracies produced by the current algorithms on the subject.

2.2. Central axis from a triangularized Circle of Willis surface

A skeletonization procedure was implemented from the discretized Willis Polygon model, starting with a triangularized surface, Fig. 4(a). The result of the vessel segmentation, Fig. 4(b), was then subjected to a *mesh* extrapolation process using the present conversion algorithm [38]. Converting a 3D logical array into an STL surface mesh (https://www.mathworks.com/matlabcentral/fileexchange/27733-converting-a-3d-logical-array-into-an-stl-surface-mesh), MATLAB Central File Exchange. Retrieved December 1, 2022), Fig. 4(c).

The geometry thus obtained was used in the processing of the corresponding central axis, after undergoing a low-intensity surface smo*othing* process to level out certain surface irregularities resulting from the triangularization algorithm. The reconstruction of the central axis was achieved through the use of a high-performance algorithm based on a Laplacian contraction model [39], Fig. 4(d).

The triangularization algorithm, with a subsequent *smoothing* step, showed a good overall result, however, with respect to the configuration of the two converging vessels, visible in the upper region of the vessel distribution, these were incorporated into a single element, leading the skeletonization function, subsequently employed, to generate a single central axis passing through that area.

The reconstruction of the central axis from discrete anatomical models, obtained from the processing of diagnostic images, suffers overall from a large margin of error relative to the inaccuracy of reconstruction of the surface of the region under examination, due to the uncertainty in the estimation of the coordinates relative to the mesh vertices. This phenomenon is highlighted above all in correspondence with small-scale elements such as a vascular reconstruction, the processing of which, in triangular format, can be highly complex from a computational point of view, with the production of results in terms of reconstructed surface area that are not always accurate. This reason has led to the consideration that the identification of the central axis starting from the interpretation of discrete geometries allows to preserve contents relating to the structural and morphological connotation of the anatomy investigated, thus guaranteeing a greater degree of accuracy in the result obtained.

2.3. Central axis from a discrete Circle of Willis surface

The applicative use of some of the most recurring center-axis reconstruction algorithms has led to results that differ somewhat depending on the level of discretization applied to the anatomical model, in line with the dimensional references common to modern diagnostic acquisition systems.

In evidence of the fact that diagnostic images suffer from a strong dependence on the degree of resolution of the tomographic machines from which they originate, a discretization algorithm has been a useful tool in verifying the effectiveness of shape analysis algorithms in varying the level of detail relative to the size of individual *voxels* and the characterization of the morphological and spatial conditions of the region under examination.

The images visible in Fig. 5(a and b) show an anatomical detail representative of the result obtained downstream of the reconstruction of the central axis in two case studies of dimensional configuration; in Fig. 5(a), the discretization was performed with a *voxel* size of 0.3 mm; in Fig. 5(b), the same size is 0.4 mm. The highlighted area denotes a common topological behaviour of the vascular branch, that is a condition of convergence, and subsequent divergence, of two branches that meet and then subsequently diverge. At the closest point, a coarse digitization of the volume leads to the generation of at least one *voxel* in common between the two branches, which results, when performing a skeletonization function, in the production of a single axis section and, consequently, a serious error in the resulting morphological characterization. Not least, it shows how the points resulting from the generation of the central axis from a discrete model, regardless of the degree of discretization involved, align with each other in a non-continuous manner, forming a

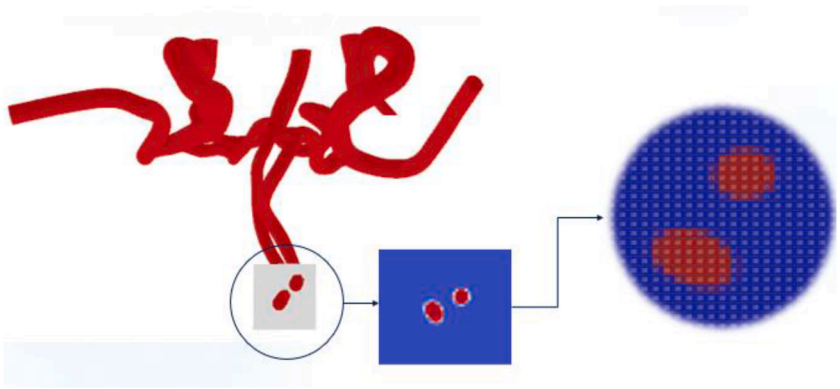

Fig. 3. Representative image of the discretization process imparted to the Willis Polygon reference model.

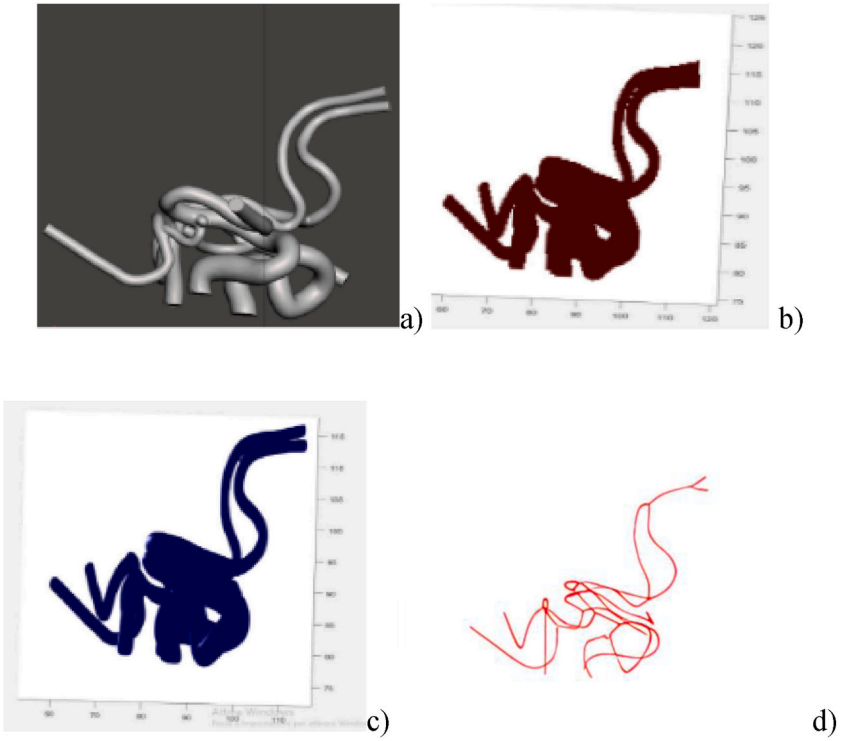

Fig. 4. Representative image of the result of the triangularization process of the Willis Polygon and subsequent reconstruction of the central axis. In (a) the ideal reconstruction model followed by that obtained by the Marching Cube algorithm (b), subsequently levelled to eliminate surface irregularities (c). In (d), the result of the reconstruction of the central axis. We highlight the error produced in the vicinity of the converging vessels where the skeleton is identified in a single section.

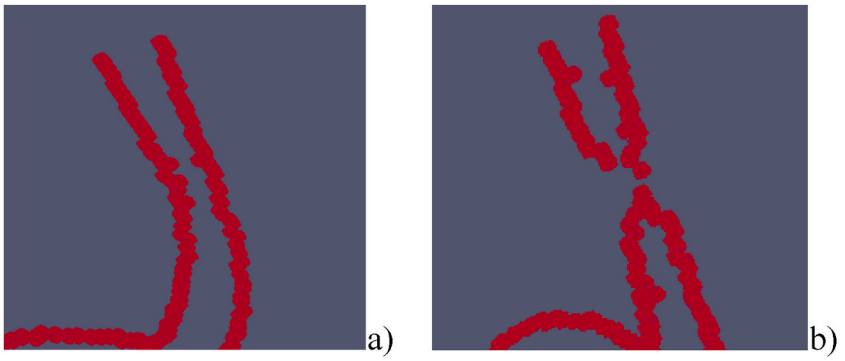

Fig. 5. Illustrative results obtained downstream of the voxel discretization process, varying the voxel size parameter from 0.3 mm, in a), to 0.4 mm, in b).

'stepped' distribution, a condition which makes it difficult to implement evaluative functions, such as the gradient, producing results that are not always accurate.

2.4. Smoothing algorithm for coordinates of center points

A critical intervention aimed at reducing the inaccuracy of the central axis reconstruction results can manifest itself through an evaluation of local intensity levels, considered on a *Hounsfield* scale, whose analysis, evaluated with respect to each point belonging to the central axis, can act as a position corrector by attracting the skeleton point to a region where a more intense radio-density value prevails.

This consideration stems from the fact that the digitization process of diagnostic machines produces a sequence of cells representative of the local radio-density level, concentrated in the cubic region, from the interpretation of which it is difficult to identify a

threshold value acting as a delimiter between two neighboring anatomical regions. The latter, consequently, will be characterized by the sharing of voxel regions, which occupy different percentages (Fig. 6).

This is the starting consideration from which we derive the importance of considering local intensity values when correcting the coordinates of the points belonging to the central axis of the anatomical region under examination. The optimization principle of the Medial Axis function, described here, is based on a smoothing algorithm applied to the coordinates of the points centered in the voxels, obtained downstream of the application of one of the skeleton-centered distance functions. The main objective is to align the points as closely as possible, eliminating the 'step' effect and facilitating the subsequent application of any subsequent anatomical investigation.

Each point of the medial axis lies on three section planes corresponding to the slices of the diagnostic acquisition process along the sagittal, axial and coronal planes. The boundaries of the vessel have shapes and dimensions depending on the arrangement of the vessel in space. For example, if the vessel section taken into consideration is aligned with the sagittal axis, the contours on the axial and coronal planes will be extremely elongated, while the contour on the sagittal plane will be almost circular (see Fig. 9).

The erosion procedure identifies the points of the medial axis approximately as centers of the minimum section, which is not necessarily oriented according to the sagittal, axial and coronal directions, not taking into account the distribution of the Hounsfield values on the contour.

Smoothing techniques based on the values adjacent to the point, such as 8-neighborhood [40], do not extend always accurately to the section boundary. Alternatively, it is possible to use the calculation of the center of gravity of the section weighted on Hounsfield values, only if the section considered coincides with the minimum section of the vessel.

If we consider, as in the previous example, the vessel with the axis aligned with the sagittal axis, the calculation of the barycentres of the contours on the axial and coronal planes will provide points that are very distant from the sagittal plane and, therefore, not significant. To understand which of the three contours is the closest to the minimum section, it is necessary to compare the dimensions of the sections.

For each point of the central axis, three axes are considered, defined as the stripes made up of all the voxels contained in the vessel along the sagittal, coronal and axial directions respectively: the longer one of the axes is compared to the others, the more reasonable it is to assume that it belongs to a plane of section not transversal to the vessel.

The basic idea is therefore to evaluate the section size along the three main directions and to separately correct the only coordinates that are believed to be representative of the cross-section centers across the vessel.

The modification of the coordinates of the points was based on a weighted average principle of the respective intensity values, expressed in *Hounsfield* scale, considered for each of the three directions. The algorithm, for each point of the central axis, processes the information relative to the intensity values of each element belonging to the *pixel* 'strip' of the cross-section area (Fig. 7.), moving horizontally, along the x-axis, vertically, along the y-axis and transversally, along the z-axis, within the anatomical region of interest, i.e. the region partitioned by the segmentation. With respect to each strip of *pixels*, the information concerning the dimensional coordinate of the *voxel* considered is re-processed on the basis of a weighted average computation, counting the respective voxels radio-density values as weights (eq. (1)) The execution process is explained in Fig. 8, in which the empty circles represent the original medial axis points located at each relative voxel center. On the basis of the weighted average computation along each directional strip considered, reiterated in all the three dimensions, the new central point location is finally replaced, represented, on the inside the image, by the filled circle. The described procedure aligns with the iterative evolution process typical of erosion algorithms, from which it draws the executive starting point. Since these are tubular bodies, differently oriented in space, the treatment of diagonal elements in the calculation of the processing of radiodensity values may incur in malformations in the definition of the spatial coordinate.

2.4.1. Critical issues considered and resolutions

The algorithm thus developed bases its procedural criterion on the computation of the weighted average over each portion of the two-dimensional vessel, iterated consecutively with respect to each of the three directions, as a function of the local intensity values, in order to return the attribution of a correct positioning of the spatial coordinates of the points of the central axis as a function of the

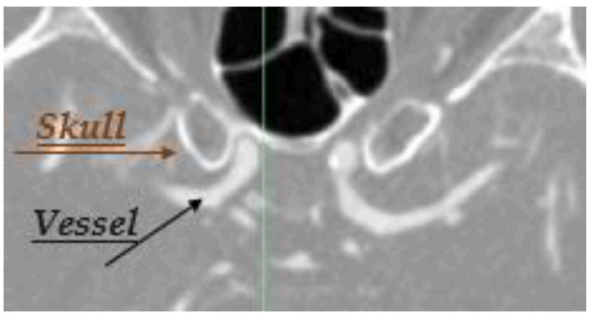

Fig. 6. Representative image of a spatial configuration of voxels belonging to a tomographic scan in which the sharing of cell volumes by two bordering anatomical regions is evident, relating to the boundary between a portion of a cerebral vessel and a cranial region. This makes it, in fact, difficult to trace a precise separation boundary between the two areas, and results in the production of inaccuracy errors in both surface reconstruction and central axis generation.

Fig. 7. Cross section area of a cerebral vessel processed by the smoothing algorithm: starting from the central axis points previously identified, located at the center of the corresponding voxel, highlighted in the yellow box, the adjacent voxel elements located along the x and y direction, marked in the blue area, are counted in computing the new central points coordinates, based on a weighted average. The procedure iterates in the remaining other directions in order to provide the new central point location, suitably smoothed.

$$x_m = \frac{\sum_{i=l}^{r} x_i h_{i00}}{\sum_{i=l}^{r} h_{i00}} \quad y_m = \frac{\sum_{j=d}^{u} y_j h_{0j0}}{\sum_{j=d}^{u} h_{0j0}} \quad z_m = \frac{\sum_{k=b}^{f} z_k h_{00k}}{\sum_{k=b}^{f} h_{00k}} \tag{1}$$

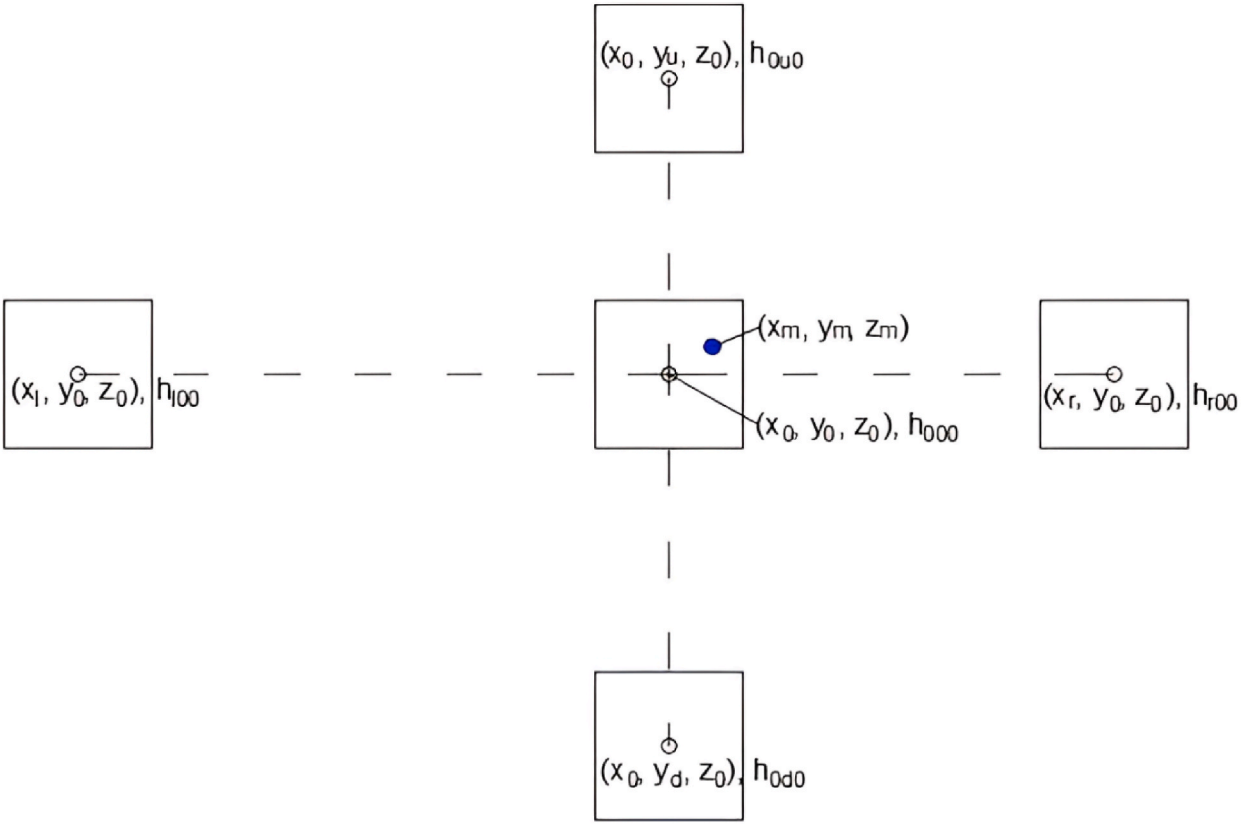

Fig. 8. Depiction scheme of the central axis smoothing procedure described. The original central point coordinates located at the center of the relative voxel, marked by the empty circle, are recomputed throughout a weighted average evaluation of the adjacent voxels of the vessel's cross section belonging area, along the horizontal and vertical directions. The procedure reiterates for all the three cross sections centered in the considered point. The algorithm returns the new x, y, and z coordinates of the central point, highlighted in the filled circle.

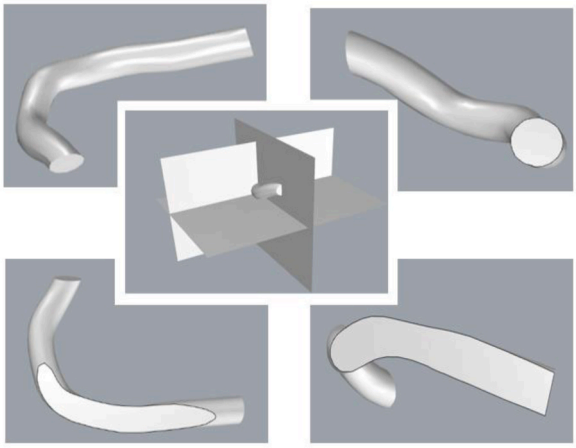

Fig. 9. Representative image of the cross sections of a vessel trait for each cutting plane considered in the three dimensions. The vessel portion considered, on the top left, is sectioned through orthogonal cutting planes along the three spatial directions, generating different section areas that result in approximated elliptical shapes. This phenomenon may incur in the generation of potential errors while computing the new spatial coordinate.

degree of attraction in percentage terms with respect to the anatomical region to which they belong.

Computational iteration on each slice through the volume of interest is performed for each direction in three-dimensional space along the *x*-, *y*- and *z-axes*, respectively. However, the vessel portion of the section under consideration may not be perfectly circular depending on the cutting plane considered, as would be expected from the section of a vascular region.

In this sense, the geometry of the section under examination may be elliptical in shape to a greater or lesser extent, a condition for which the process of reconstructing the central axis, thus described, may incur in errors in the formulation of the new nodal co-ordinates for at least two of the three coordinates (Fig. 9). To remedy this, the following verification conditions were implemented, through the identification of two control parameters, suitably optimized:

- If the new co-ordinate, for each axis considered, is distant from the original one with respect to a neighboring range of values, then this may represent an error in the arrangement of the correct point. An illustrative case of the condition under consideration may occur when the vessel cut section is similar to that shown in Fig. 10., where the weighted average over the nodal coordinates produces, for each successive cut direction along a considered direction, z_n *and* z_{n+1} a sequence of nodes aligned in space next to each other.

  In this condition, given a threshold value 'Delta', the *voxel under* examination is not subjected to the correction process.

- If, on the other hand, the weighted averages are not affected by the criticality described, a dimensional check is carried out between the size S_i of the section considered and the minimum size between S_1, S_2 and S_3, so as to ensure proportionality of the dimensions of each section (Fig. 11). This check is necessary where the sectioning of the considered vessel section generates an oblique element, which is deformed in width with reference to the other two cutting planes.

In this second check, the 'Threshold' parameter is introduced as a discriminating element, capable of correcting any deviation of the new co-ordinate from the centered reference point.

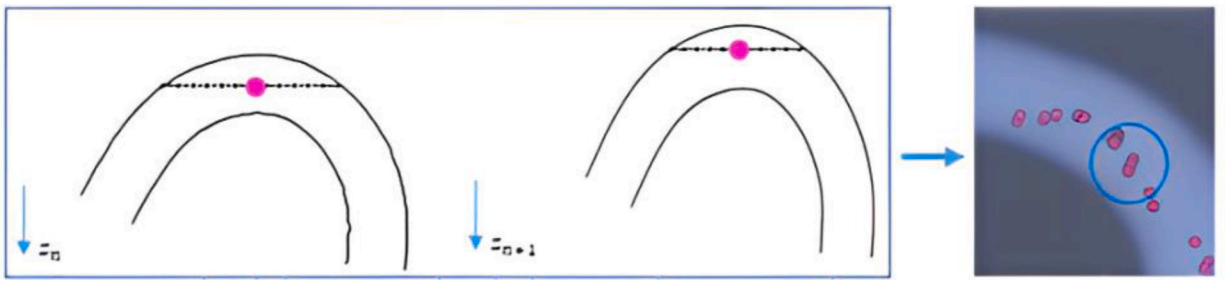

Fig. 10. Graphical representation of two cutting sequences along a spatial direction in which a critical condition is generated by the central axis correction process. Along the cut direction considered, the section produced, oblique to the actual cross-section of the vessel, for each spatial plane considered produces a new co-ordinate, returning a sequence of points in space aligned with respect to one direction.

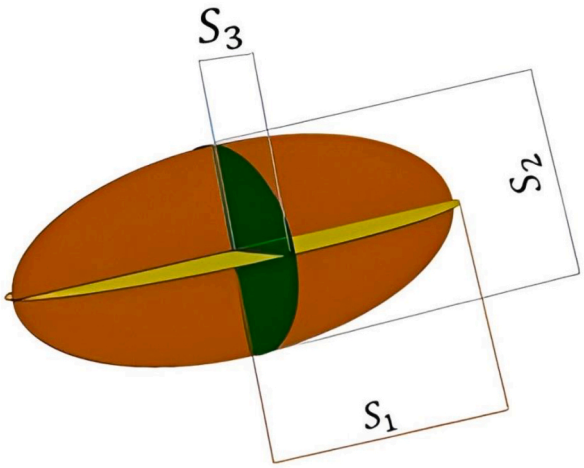

Fig. 11. Representative image of a condition of dimensional irregularity of the three cutting sections developed for the element under examination along the three dimensions. The dimensional deviation of a cutting section above a 'Threshold' value can generate obvious errors in the processing of the new co-ordinates of the central axis, which is why the condition shown is not subjected to the corrective calculation described.

An optimization checking of the two discriminating parameters 'Delta' and 'Threshold', respectively, made it possible to obviate the presence of reconstruction inaccuracies, where present, by returning a uniform arrangement of the nodes relative to the central axis, appropriately aligned and ordered in sequential form. A visual representation of the described procedure is shown in Fig. 12(a and b) in which parallelly compared the original central points' displacement, Fig. 12(a), with the corrected realignment outcome from the smoothing effect, Fig. 12(b).

3. Results

The optimization process of the identified criticality parameters, *Delta* and *Threshold*, was obtained on the basis of a computational processing concerning the minimization of the sum of the distance between the consecutive points of each identified stretch. The criterion adopted is represented by the fact that the alignment of the points of the central axis is measurable through the minimization of the overall length. The starting length computed on the original medial axis before the application of the smoothing algorithm corresponds to 201.0 voxel fraction. The target length computed with respect of the triangularized central axis regarded as a reference GoldStandard in the uniformly disposal of the central points is 108.4 voxel fraction. This measurement is, however, inevitably slightly underestimated due to the errors highlighted in the comment related to the figure Fig. 4(d). In Table 1, we report the experimental results calculated as a function of a specific section of the vascular branch, overall the longest one identified, oriented transversely in three-dimensional space. The optimization process thus described returned an accurately aligned sequential ordering of the central axis points, the graphical result of which can be observed in Fig. 13(a–c).

The identified minimum condition corresponds to specific combination values of the parameters Delta and Threshold.

In Table 2, we show the results obtained when the Delta and Threshold parameters investigated vary. More in detail, the condition of minimum optimum results in the generation of a single vessel element, Fig. 13(b), a fundamental condition in guaranteeing the presence of a high margin of continuity between the nodes of the central axis. Too high values of the Delta and Threshold parameters, on the other hand, identify the conformation of the vessel portion as consisting of an agglomeration of several elements, resulting in an overall jagged and disconnected geometry, as highlighted in Fig. 13(c).

Fig. 14 shows a visual comparison, obtained by superposition, between the distribution of points on the central axis originating from the use of the traditional functions described above, and the distribution of points modified according to neighboring threshold values, highlighted in red. The optimization function was in fact able to redistribute the points in a more orderly and sequential manner, largely cancelling out the scaled conformation due to the discrete distribution of the spatial model considered. It can be seen that the process of optimizing the central axis was extremely effective in rearranging the sequence of points, continuously orienting them in an orderly manner.

The application of the algorithm produced a medial axis whose overall length, without optimization of the parameters *delta* and *threshold*, was reduced by 31.8 % compared to the initial length. This variation denotes a significant reduction in the stepped effect.

The analysis of the influence of the delta and threshold values highlighted an improvement of another 7 %, obtaining a final reduction of 38.8 %. The measurement obtained in the optimal combination of delta and threshold values is quite close to the target measurement, with a difference percentage of around 13.3 %. Too high values of the threshold cause a fragmentation of the sections, leading some center points to coincide and must therefore be avoided. Future developments include the application of the algorithm to a sufficient number of skull circulatory systems and the implementation of controls on the relative inclination between successive center points to reduce the negative effects of delta and threshold.

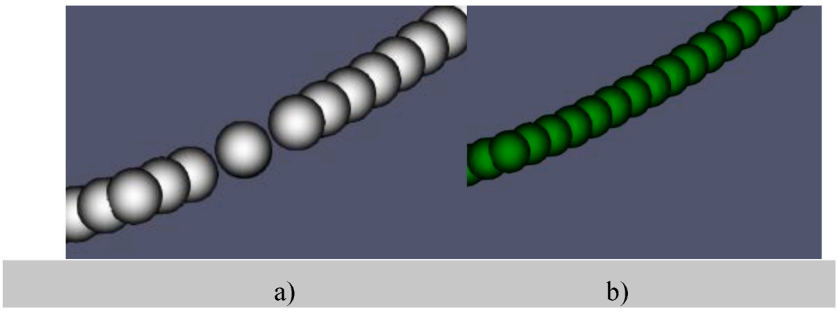

Fig. 12. In a), the original medial axis central points location; in b), the central realignment resulingt from the optimization process of the smoothing algorithm, through the identification of threshold values for the appropriate 'Threshold' and 'Delta' parameters.

Table 1
A representative table of the overall distance values identified when varying the Delta and Threshold parameters.

	Threshold							
		1.0	*1.3*	*1.5*	*1.7*	*2.0*	*2.5*	*3.0*
Delta	*0.5*	137.713	136.383	136.510	136.530	136.580	136.615	136.615
	1.0	137.713	127.184	126.970	126.979	127.059	127.256	136.615
	1.3	137.713	122.462	122.163	122.207	122.735	123.810	124.044
	1.7	137.713	122.462	122.163	122.856	123.862	125.341	125.575
	2.0	137.713	122.462	122.163	122.856	123.862	126.027	126.434
	3.0	137.713	122.462	124.236	122.856	125.935	131.093	131.915
	5.0	137.713	122.462	124.236	122.856	125.935	131.093	132.663
	7.0	137.713	122.462	124.236	122.856	125.935	140.858	151.964

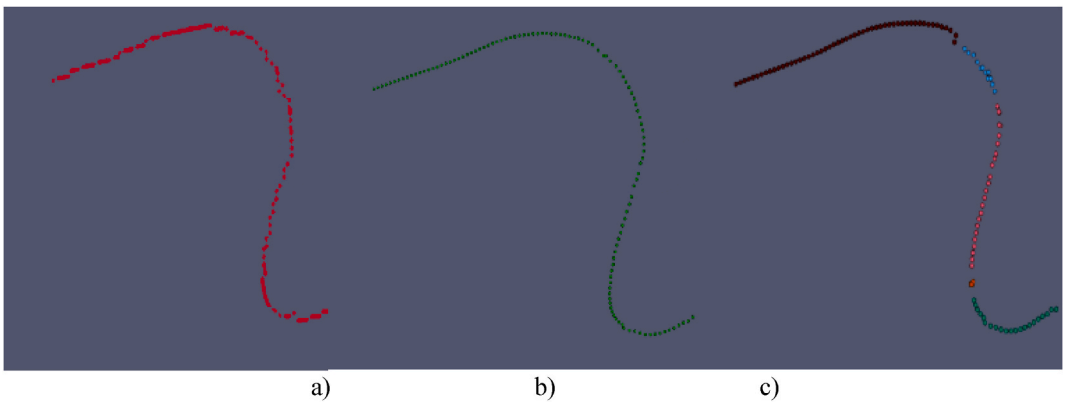

Fig. 13. Representative image of the central axis smoothing result obtained. In a), the original central axis referred to a vessel; in b) the smoothing result obtained downstream of the optimization process of the Delta and Threshold parameters; in c) the result in the worst case where the same portion of the vessel is the result of several strokes together.

4. Conclusions

The purpose of this method is to improve the medial axis reconstruction results from the traditional mathematical functions usually applied to discrete anatomical element deriving from diagnostic investigations, by manipulating its central points' position, reconsidering the information regarding the Hounsfield Scale radiodensity value of the voxels belonging to each slicing section considered, normally lost after the segmentation procedure. To state this purpose, we considered the entire vessels ramification belonging to the cerebral Circle of Willis, assigning it the property of contemplating the majority of the typical topological and morphological drawbacks usually pertained to the field of anatomical reconstruction, i.e. small-scale dimensions, rangeability of curvature and orientation and tortuosity variations.

The processing of diagnostic images inevitably produces shape irregularities due to the discretized condition of digital images. This can affect the extrapolation of dimensional information characterizing the morphology of the anatomy under examination, which is fundamental in clinical examination. Among the most commonly used processing functions, the reconstruction of the central axis

Table 2
Table representing the number of elements that make up the processed vessel section. The optimal condition is represented by the production of a single, continuous and regular vessel tract.

	Threshold						
		1.0	*1.3*	*1.5*	*1.7*	*2.0*	*2.5*	*3.0*
Delta	*0.5*	*0*	*0*	*0*	*0*	*0*	*0*	*0*
	1.0	*0*	*0*	*0*	*0*	*0*	*0*	*0*
	1.3	*0*	*0*	*0*	*0*	*0*	*0*	*0*
	1.7	*0*	*0*	*0*	*0*	*1*	*5*	*5*
	2.0	*0*	*0*	*0*	*0*	*1*	*2*	*4*
	3.0	*0*	*0*	*0*	*0*	*1*	*2*	*5*
	5.0	*0*	*0*	*0*	*0*	*1*	*6*	*8*
	7.0	*0*	*0*	*0*	*0*	*1*	*7*	*8*

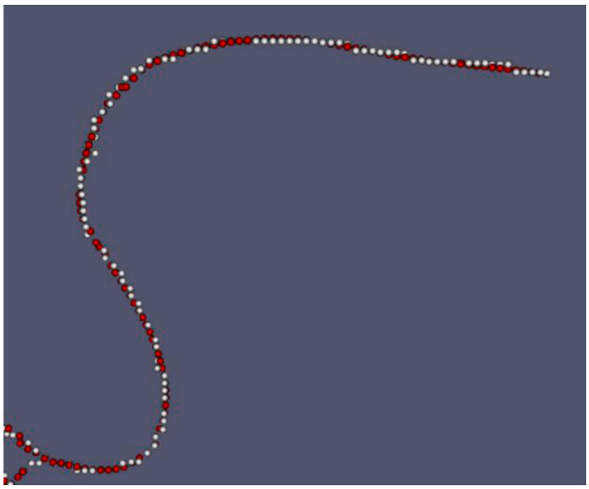

Fig. 14. Representative image of the result of the smoothing algorithm applied to the central axis. The original skeleton, visible in white, has been modified by cancelling the step effect, resulting in an alignment of the points, in red.

represents the most widespread tool through which dimensional calculations can be simplified. The objective of this research study was to reconstruct the central axis passing through a vascular branch, reconstructed from diagnostic investigations, starting from a corrective process of the results produced by some of the most widespread algorithms for processing central axes for diagnostic applications, normally affected by a spatial connotation of a granular type, with evident irregularities in shape, due to the volume discretization that characterizes digital images. An optimization algorithm is, therefore, proposed, capable of producing a realignment of the axis points, which are thus reordered and uniformly and regularly shaped. To do this, an algorithmic system of weighted control of the local intensity levels of the adjacent voxels, representative of the radio-density level, is implemented in order to center the nodal placement according to the anatomical weight of the region affected by the central axis reconstruction.

Obtaining an axis element that is effectively centered with respect to the reference anatomy represents a fundamental starting point in the elaboration of accurate morphological investigations from which to deduce the identification of alterations of a pathological nature, where present, from the scanning of diagnostic investigations. The proposed algorithm can also represent a valid tool in the drafting of algorithmic procedures to be implemented within modern software instruments for clinical use.

Data availability statement

Data will be made available on request.

CRediT authorship contribution statement

C. Fontana: Writing – review & editing, Writing – original draft, Visualization, Validation, Software, Investigation, Formal analysis, Data curation, Conceptualization. **N. Cappetti:** Writing – review & editing, Writing – original draft, Visualization, Validation, Supervision, Methodology, Formal analysis, Data curation, Conceptualization.

Declaration of competing interest

The authors declare that they have no known competing financial interests or personal relationships that could have appeared to influence the work reported in this paper.

References

[1] G. Zwettler, R. Swoboda, F. Pfeifer, W. Backfrieder, Fast medial axis extraction algorithm on tubular large 3D data by randomized erosion, in: Communications in Computer and Information Science, 2009, https://doi.org/10.1007/978-3-642-10226-4_8.

[2] S. Sultana, J.E. Blatt, B. Gilles, T. Rashid, M.A. Audette, MRI-based medial Axis extraction and boundary segmentation of cranial nerves through discrete deformable 3D contour and surface models, IEEE Trans. Med. Imag. 36 (8) (2017), https://doi.org/10.1109/TMI.2017.2693182.

[3] J.H. Noble, B.M. Dawant, An atlas-navigated optimal medial axis and deformable model algorithm (NOMAD) for the segmentation of the optic nerves and chiasm in MR and CT images, Med. Image Anal. 15 (6) (2011), https://doi.org/10.1016/j.media.2011.05.001.

[4] C. Fetita, et al., Transferring CT Image Biomarkers from Fibrosing Idiopathic Interstitial Pneumonia to COVID-19 Analysis, 2021, https://doi.org/10.1117/12.2580658.

[5] D. Ding, Z. Pan, D. Cuiuri, H. Li, N. Larkin, Adaptive path planning for wire-feed additive manufacturing using medial axis transformation, J. Clean. Prod. 133 (2016), https://doi.org/10.1016/j.jclepro.2016.06.036.

[6] M. Fu, R. Liu, B. Qi, R.R. Issa, Generating straight skeleton-based navigation networks with Industry Foundation Classes for indoor way-finding, Autom. ConStruct. 112 (2020), https://doi.org/10.1016/j.autcon.2019.103057.

[7] A. Nouri, et al., Characterization of 3D bifurcations in micro-scan and MRA-TOF images of cerebral vasculature for prediction of intra-cranial aneurysms, Comput. Med. Imag. Graph. 84 (2020), https://doi.org/10.1016/j.compmedimag.2020.101751.

[8] C.Y. Lin, Y.T. Ching, Extraction of coronary arterial tree using cine X-ray angiograms, Biomed. Eng. 17 (3) (2005), https://doi.org/10.4015/S1016237205000184.

[9] J. Yang, P.T. Gonzalez-Bellido, H. Peng, A Distance-Field Based Automatic Neuron Tracing Method, 2013.

[10] H. Zou, W. Zhang, Q. Wang, An improved cerebral vessel extraction method for MRA images, Bio Med. Mater. Eng. 26 (2015) S1231–S1240, https://doi.org/10.3233/BME-151420.

[11] Y. Wang et al., "Deep Distance Transform for Tubular Structure Segmentation in CT Scans."..

[12] M. Kazemi, L. Wecker, F. Samavati, Efficient calculation of distance transform on discrete global grid systems, ISPRS Int. J. Geo-Inf. 11 (6) (Jun. 2022), https://doi.org/10.3390/ijgi11060322.

[13] P.K. Saha, R. Strand, G. Borgefors, Digital topology and geometry in medical imaging: a survey, IEEE Trans. Med. Imag. 34 (9) (2015), https://doi.org/10.1109/TMI.2015.2417112.

[14] H. Blum, "1967-blum.pdf," Models for the Perception of Speech and Visual Form, 1967.

[15] L. Liu, E.W. Chambers, D. Letscher, T. Ju, Extended grassfire transform on medial axes of 2D shapes, CAD Computer Aided Design 43 (11) (2011), https://doi.org/10.1016/j.cad.2011.09.002.

[16] Q.J. Wu, J.D. Bourland, R.A. Robb, <title>Fast 3D medial axis transformation to reduce computation and complexity in radiosurgery treatment planning</title&gt, in: Medical Imaging 1996: Image Processing, 1996, https://doi.org/10.1117/12.237959.

[17] E. Bertin, F. Parazza, J.M. Chassery, Segmentation and measurement based on 3D Voronoi diagram: application to confocal microscopy, Comput. Med. Imag. Graph. 17 (3) (1993), https://doi.org/10.1016/0895-6111(93)90041-K.

[18] C. Lin, et al., SEG-MAT: 3D shape segmentation using medial Axis transform, IEEE Trans. Vis. Comput. Graph. 28 (6) (2022), https://doi.org/10.1109/TVCG.2020.3032566.

[19] Transactions on large-scale data- and knowledge-centered systems III - special issue on data and knowledge management in grid and P2P systems, Lect. Notes Comput. Sci. 6790 (LNCS) (2011).

[20] N. Sharma, D. Ostas, H. Rotar, P. Brantner, F.M. Thieringer, Design and additive manufacturing of a biomimetic customized cranial implant based on Voronoi diagram, Front. Physiol. 12 (2021), https://doi.org/10.3389/fphys.2021.647923.

[21] J.W. Brandt, V.R. Algazi, Continuous skeleton computation by Voronoi diagram, CVGIP Image Underst. 55 (3) (1992), https://doi.org/10.1016/1049-9660(92)90030-7.

[22] R.L. Ogniewicz, O. Kübler, Hierarchic Voronoi skeletons, Pattern Recognit 28 (3) (1995), https://doi.org/10.1016/0031-3203(94)00105-U.

[23] M. Schmitt, Some examples of algorithms analysis in computational geometry by means of mathematical morphological techniques, in: Lecture Notes in Computer Science (Including Subseries Lecture Notes in Artificial Intelligence and Lecture Notes in Bioinformatics), 1989, https://doi.org/10.1007/3-540-51683-2_33.

[24] A. Tagliasacchi, T. Delame, M. Spagnuolo, N. Amenta, A. Telea, 3D skeletons: a state-of-the-art report, Comput. Graph. Forum (2016), https://doi.org/10.1111/cgf.12865.

[25] Y.F. Tsao, K.S. Fu, A parallel thinning algorithm for 3-D pictures, Comput. Graph. Image Process. 17 (4) (1981), https://doi.org/10.1016/0146-664X(81)90011-3.

[26] C. Santarelli, L. Puggelli, Y. Volpe, P. Serio, R. Furferi, A semiautomatic procedure to assist physicians in paediatric airway stenting, in: Lecture Notes in Mechanical Engineering, 2023, https://doi.org/10.1007/978-3-031-15928-2_15.

[27] G. Bertrand, M. Couprie, Parallel skeletonization algorithms in the cubic grid based on critical kernels, in: Skeletonization: Theory, Methods and Applications, 2017, https://doi.org/10.1016/B978-0-08-101291-8.00008-0.

[28] G. Németh, P. Kardos, K. Palágyi, Thinning combined with iteration-by-iteration smoothing for 3D binary images, in: Graphical Models, 2011, https://doi.org/10.1016/j.gmod.2011.02.001.

[29] C. Arcelli, G.S. Di Baja, A width-independent fast thinning algorithm, IEEE Trans. Pattern Anal. Mach. Intell. PAMI-7 (4) (2009), https://doi.org/10.1109/tpami.1985.4767685.

[30] J.-I. Toriwaki and K. Mori, "Distance Transformation and Skeletonization of 3D Pictures and Their Applications to Medical Images."..

[31] F.L. Yuan, Combined 3D thinning and greedy algorithm to approximate realistic particles with corrected mechanical properties, Granul. Matter 21 (2) (2019), https://doi.org/10.1007/s10035-019-0874-x.

[32] W.E. Lorensen, H.E. Cline, Computer graphics, volume 21, number 4, July 1987, marching cubes: a high resolution 3D surface construction algorithm, ACM siggraph computer graphics 21 (4) (1987).

[33] A. Nouri, et al., Characterization of 3D bifurcations in micro-scan and MRA-TOF images of cerebral vasculature for prediction of intra-cranial aneurysms, Comput. Med. Imag. Graph. 84 (2020), https://doi.org/10.1016/j.compmedimag.2020.101751.

[34] D. Shaked, A.M. Bruckstein, Pruning medial axes, Comput. Vis. Image Understand. 69 (2) (1998), https://doi.org/10.1006/cviu.1997.0598.

[35] A.D. Ward, G. Hamarneh, The groupwise medial axis transform for fuzzy skeletonization and pruning, IEEE Trans. Pattern Anal. Mach. Intell. 32 (6) (2010), https://doi.org/10.1109/TPAMI.2009.81.

[36] N. Wilson, K. Wang, R.W. Dutton, C. Taylor, A software framework for creating patient specific geometric models from medical imaging data for simulation based medical planning ofvascular surgery, in: Lecture Notes in Computer Science (Including Subseries Lecture Notes in Artificial Intelligence and Lecture Notes in Bioinformatics), 2001, https://doi.org/10.1007/3-540-45468-3_54.

[37] R. Van Uitert, I. Bitter, Subvoxel precise skeletons of volumetric data based on fast marching methods, Med. Phys. 34 (2) (2007), https://doi.org/10.1118/1.2409238.

[38] A. Hilbert, et al., Anatomical labeling of intracranial arteries with deep learning in patients with cerebrovascular disease, Front. Neurol. 13 (2022), https://doi.org/10.3389/fneur.2022.1000914.
[39] J. Cao, A. Tagliasacchiy, M. Olsony, H. Zhangy, Z. Su, Point cloud skeletons via Laplacian-based contraction, in: SMI 2010 - International Conference on Shape Modeling and Applications, Proceedings, 2010, https://doi.org/10.1109/SMI.2010.25.
[40] W. Deng, S.S. Iyengar, N.E. Brener, Fast parallel thinning algorithm for the binary image skeletonization, Int. J. High Perform. Comput. Appl. 14 (1) (2000), https://doi.org/10.1177/109434200001400105.